Joining TWIP to TWIP and TWIP to Aluminium: a comparative study between joining processes, joint properties and mechanical performance

I. Papadimitriou[1], P. Efthymiadis[1], H.R. Kotadia[1], I. R. Sohn[2], S. Sridhar[1]

[1]*Warwick Manufacturing Group*, The University of Warwick, Coventry, CV4 7AL, UK
[2] *POSCO research labs*, 8, Pokposarang-gil, Gwangyang-si, Jeonnam, 545-875, South Korea

[*]*Corresponding author: Y.Papadimitrious@warwick.ac.uk, Tel: 0044 (0) 2476572528*

Abstract:

In the present study, Resistance Spot Welding (RSW), Self-Piercing Riveting (SPR), Kerb Konus Riveting (KKR) and EJOWELD techniques were investigated for joining of TWIP steel sheets with one another and with Al. This is the first time the KKR and EJOWELD methods were compared to conventional joining methods. The main focus was on the mechanical properties of similar joints produced between Zn-coated Fe–12Mn–1.5Al–1Si–0.5C Twinning Induced Plasticity (TWIP) steel and dissimilar joints between Zn-coated TWIP and Al 5754 or Al 6111 aluminium alloy sheet. The nugget solidification after fusion welding was evaluated through characterization with SEM-EBSD. In the case of RSW produced joints it was found that the joints with smaller grain size and larger orientation diversity exhibited larger maximum load capability. Regarding the joints produced with the EJOWELD method, grain size did not vary much compared with the base metal. Mechanical properties and the fracture behaviour of these joints were identified through the application of the lap shear method and failure modes. In the case of TWIP/TWIP combination, the results demonstrated that RSW samples exhibited the highest maximum load and maximum elongation, while in dissimilar joining SPR exhibited the largest maximum load. The EJOWELD method for the dissimilar joints showed similar mechanical properties to the SPR, in terms of maximum load, while KKR poorer properties. By comparing the mechanical properties of all the joints, it can be concluded that the primary factor of joint strength in RSW were the joining parameters (preweld and number of weld currents, welding time), while in the case of the other techniques it was the sheet strength.

Keywords: Twinning-induced-plasticity (TWIP) steel; Wrought aluminium alloys; Resistance Spot Welding (RSW); Self-Piercing Riveting (SPR); EJOWELD friction-stir welding; Kerb-Konus Tuk rivet; Mechanical properties.

1. Introduction

Weight reduction of vehicles has become an important issue in order to meet fuel efficiency standards such as Corporate Average Fuel Economy (CAFE) [1] in the US and the EU emission standards [2]. This has led to the application of lighter materials than conventional steels, such as Advanced High Strength Steels (AHSS), aluminium and composites. Fuel consumption, emissions, comfort and safety without compromising performance can be achieved by the use of aluminium alloys in the Body in White (BIW) [3-6]. There are at least three ways to decrease the weight of a vehicle: (i) reduce its size, (ii) optimise its design, and (iii) replace materials used in its construction with lighter mass equivalents. The third option, use of lightweight materials, has been pursued to a greater extent [1-4]. Aluminium alloys can be beneficial in terms of forming, corrosion resistance, crashworthiness as well as recyclability. In order to optimise automotive structures of the future, multi-material structures will likely constitute a solution wherein joining will be challenge. Joining has always been a crucial part of the car design and in order for the aluminium alloys to be used in the automotive industry, and joinability of AHSS to Al remains a challenge.

A significant proportion of this effort is currently being directed toward the substitution of steel for aluminium in the body structure (the body accounts for 20–25% of the total weight of the vehicle) [7]. The AA 5754 and 6111 are two different grades of aluminium designed for different uses in the automotive industry [8]. Alloys of the 5xxx (Al - Mg) series have been considered for use in structural automotive components in North America [9], while alloys of the 6xxx series (Al-Mg-Si) have been considered for use as skin materials. Currently, the highly formable 5xxx alloys are used primarily for inner panel applications, whilst the heat-treatable 6xxx alloys are preferred for outer panel applications.

High strength steels have been used extensively in the automotive industry so that safer, more environmentally friendly and impact resistant vehicle design can be achieved. High manganese austenitic steels are a promising candidate for automotive body structure components owing to their high tensile strength, large ductility and exceptional work-hardening rate. Owing to the stacking fault energy (SFE) of TWIP steels (20 to 45 mJm^{-2}), these properties are a result of a competing classical dislocation glide mechanism with the twinning deformation mode, known as the twinning-induced-plasticity (TWIP) effect [10-12]. Prerequisites for achieving the substitution of the steels used nowadays in BIW with TWIP in high volume production are robust joining methods. One of the major challenges of joining TWIP steels has been the detrimental effect of Zn, causing Liquid Metal Embrittlement (LME) and subsequently joints with poorer mechanical properties [13]. On the other hand, SPR does not involve liquid Zn formation and can avoid this, but is limited in terms of access. When joining steels to Al through methods that require heating, a further materials related barrier is caused by the formation of Fe-Al intermetallic phases that may cause brittleness [14].

Resistance spot welding (RSW) of steel is currently the dominant conventional joining method for the BIW in the automotive industry [15]. The primary benefits of RSW are high speed and low cost operation (especially in the case of similar steel sheet joining) and the ability to use the same facility for a wide range of configurations. In the case of aluminium joining however, it reaches limitations such as consistency and electrode life [16, 17].

Self-piercing riveting (SPR) is another production process used to join similar (aluminium to aluminium) and dissimilar (steel to aluminium) sheet body structures [18, 19]. The tubular rivet tail flares-out and interlocks the sheets inside a button formed part of the lower sheet. One advantage of this technique over RSW is that it is not a fusion process and therefore no fume emissions, phase transformations or melting/solidification that can result in brittle-phase formation and hot cracking through liquid metal embrittlement (LME) cracking. Regarding the LME challenge of the Zn-coated materials, it has been reported that the peak temperature of the process is approximately 125 ^{o}C, whereas the melting temperature of Zn is well above (419.5 ^{o}C) [20]. Also, SPR has no pre-drilled hole requirement. However, with SPR there is the inability of quick process parameters change (such as rivet size or die configuration) between successive joint positions, a property where RSW has a clear advantage. Furthermore, the steel rivets currently used not only don't benefit the recyclability of the BIW assembly but they also add to its weight and cost.

Solid punch riveting or Kerb Konus riveting (KKR) [21] is a process different to the punch riveting in that the rivet is punched through both sheets to be joined. One advantage of this process is that apart from coated stainless steel rivets, aluminium rivets can also be used. The advantages of this method are that it benefits the weight reduction of the BIW and its recyclability. However, the strength of the produced joint is inferior of that produced with SPR.

Lastly, EJOWELD [22] is a friction stir welding technique used for multi material joining. The process's benefits are that it is a relatively fast process (completed in under a second) and does not create any sparks or flash, while localising heat generation, limiting diffusion times to avoid formation of un-wanted phases. To the best of the authors' knowledge this is the first study in which the KKR and EJOWELD methods are included and compared with conventional joining methods.

The aim of the present study is to investigate the joinability of TWIP steels and to compare four joining processes (RSW, SPR, KKR and EJOWELD) for the TWIP/Al 5754, TWIP/Al 6111 and TWIP/TWIP configurations on the basis of joint strength and elongation. To the best of the authors' knowledge a comparative review of the above methods from producing similar and dissimilar TWIP steel and Al 5754 or Al 6111 has not been carried out.

2. **Experimental**

2.1. Materials

The steel sheet investigated in this work is the TWIP900 steel samples were received in sheet form with 1.12mm thickness from POSCO. The chemical composition of the studied material was Fe–12Mn–1.5Al–1Si–0.5C. All compositions in this article are given in weight percent unless otherwise stated. The sheets were Zn-coated with a coating thickness of 10 μm. The investigated TWIP steel is fully austenitic and does not show any phase transformation in the temperature range from 420 to 1000 ^{0}C [23]. The microstructure of the base material can be seen in Fig. 1. The sheet thicknesses of the Al 5754 (Al-0.3Si-0.3Fe-0.1Cu-0.5Mn-0.3Mg) and Al 6111 (Al-0.75Mg-0.85Si-0.7Cu-0.25Fe-0.3Mn) were 2 and 1.2 mm, respectively. The reason the former thickness is that larger than the latter, is that in the automotive industry the Al 5754 is used for the body-in-white (BIW), while Al 6111 is mostly used as a skin alloy.

2.2. Joining techniques

The RSW was carried out on a medium frequency DC (MFDC) inverter TECNA 3650 spot welder with a 6 mm tip diameter of Cu dome radius electrode under a constant cooling of 6 l/min. The materials combination that was produced by spot welding was limited to TWIP/TWIP since the dissimilar joints were not possible due to the challenges introduced by aluminium. Primarily, the high thermal and electric conductivity would have resulted in three times higher welding current requirement which was deemed unreasonable.

Welding current and time are the main process parameters. These two parameters that controls weld nugget microstructural evolution and the subsequent mechanical behaviour is heat input. During the welding, the heat input is mainly controlled by current, time and electrical resistance of the steels. The heat input can be expressed as,

$$Q = tRI^2 \quad (1)$$

where Q and R express the heat input and the bulk resistance, respectively. I represents the welding current and t the welding time.

After optimising the process with respect to cracking, two different welds were produced by the welding cycle profiles depicted in Fig. 2. The main difference between the two was the total welding time as the profile A was produced in slightly less time than one second and profile B in approximately 1.5 seconds (as a pre-weld current and 2 separate weld currents along with a slope-up and slope-down was introduced to the latter). Specifically, profile B was selected with regard to minimal Zn embrittlement and subsequent LME cracking occurrence [24].

The system where the SPR joining was carried out can be seen in Fig. 3 (a). The combinations that were produced were TWIP/Al 5754 and TWIP/Al 6111 whereas the TWIP/TWIP could not be produced since the hardness of the TWIP bottom layer would cause the rivet leg to not flare sufficiently, buckle, bend and/or fracture (Fig. 3 (b)). Dies for SPR can have a cavity with a flat bottom or a pip in the middle

with different geometries and dimensions. A R-shaped die (die with a pip) can increase the interlock distance and enhance rivet deformation, but it will also introduce larger plastic deformation of the bottom sheet and will require a larger setting force [25]. The dies selected for the present study had a pip in the middle. The process was controlled by head height which was -1.3 mm for TWIP/Al 5754 and -1.6 mm for TWIP/Al 6111. The clamping force was 5kN and the initial velocity 60 mm/s. A steel H4 rivet with a radius of 5mm each was used. Its rivet length was selected to be 5.3 mm based on the guideline by Henrob, Ltd who suggest that for a 5 mm diameter rivet, the rivet length should be 2-4 mm longer than the stack thickness. In both cases the TWIP sheet was at the top, while the Al sheet was at the bottom.

The KKR process can be seen in Fig. 4. The rivet is punched through the sheets (Fig. 4 (c)), substituting the corresponding sheet material (Fig. 4 (d)). Afterwards, force is applied to the lower part of the bottom sheet (Fig. 4 (e)), causing it to plastically deform (Fig. 4 (f)). The press-in force is a parameter that depends mostly on the sheet strength and after optimising the process, the force used was 29 kN. The top layer was the TWIP steel, while the Al was the bottom sheet in both cases. All three configurations were produced with this process.

The EJOWELD process can be seen in Fig. 5. It is a four key-stage process where in the first stage the component pierces the top layer (Fig. 5 (a)) and then by revolving at high speeds (Fig. 5 (b,c)) under-fills the materials to be joined (Fig. 5 (d)). The component that was used consisted of steel resistant steel, while the starting axial force was 9 kN and the head rotation speed was approximately 2000 RPM. The combinations that were carried out were TWIP/Al 5754 and TWIP/Al 6111 as for the TWIP/TWIP combination a pre-drilling was required due to the TWIP steel's hardness.

The general process parameters of the techniques under study are summarised in Table 1. Joining of TWIP to TWIP was feasible with RSW and KKR processes, while joining of TWIP to Aluminium was only successful for SPR, KKR and EJOWELD. The smallest force was applied in the case of RSW, due to the fact that it is a fusion process and does not include any riveting, drilling or punching. In the other three riveting processes, the force increases as one moves from EJOWELD, to KKR, to SPR. EJOWELD requires the lowest force of all three riveting processes due to the revolution of the rivet. The overall fastest process was RSW, while from the three riveting processes, SPR was the fastest.

Table 1. Main process parameters for the techniques under study.

Joining technique	Similar	Dissimilar	Force	Process time
RSW	✓	Too high current required	2.8 kN (electrode)	1-1.5 s

SPR	Very hard rivet required	✓	~60 kN (maximum)	1-4 s
KKR	✓	✓	29 kN (press-in)	2-4 s
EJOWELD	Pre-drilling required	✓	9 kN (drilling)	2.6 s

1

2

3 2.3. Post joining characterisation

4 The mechanical behaviour of the welded joints was investigated by lap shear testing with an INSTRON
5 30kN universal testing machine. Every set of joining combination consisted of three separate joints in
6 order to ensure the reliability of the results. The highest standard deviation was observed for the RSW
7 joints (322 N). Lap shear testing was carried out at a strain rate of 5×10^{-3} s^{-1}. Each lap shear test
8 specimen consisted of two pieces measuring 125 mm × 38 mm, with a 38 mm overlap according to the
9 AWS D8 (Fig. 6). Samples for microstructural examination were cut from the vertical cross section of
10 the weld nugget and mounted in Bakelite. The mounted specimens were ground using standard
11 techniques with SiC abrasive papers of different grit and polished with 1 and 0.25 μm silica suspension
12 solutions. Microstructure characterisation for the preliminary study observation was performed using a
13 Nikon stereo optical microscope (OM). A Zeiss Sigma field emission scanning electron microscope
14 (SEM) equipped with energy-dispersive X-ray spectroscopy (EDX) and Electron Backscatter
15 Diffraction (EBSD) was used at 30 kV operating voltage for detail microstructure analysis such phase
16 identification, texture evolution etc. For EBSD analysis specimen was tilted to 70° from the horizontal
17 and 2 μm step size was used for all specimens.

18 **3. Results**

19 The results are focused on the successful joints, presented in Table 1, and how they performed in terms
20 of mechanical tests and post-characterization analysis.

21 3.1. Joints produced through Resistance Spot Welding (RSW)

22 An EBSD micrograph from the supplied TWIP steel is presented in Fig. 1 illustrating the overall
23 microstructure and presence of the austenitic grain. The two Inverse Pole Figures in Fig. 7 depict the
24 weld nuggets produced by two distinctive welding profiles A (Fig. 7 (a)) and B (Fig. 7 (b)). A substantial
25 difference in terms of grain size and grain orientation diversity was evident between the two specimens.
26 Quality and structure of the weld nugget have been known to be dependent of the heating and melting
27 processes. Furthermore, the strength of the joint depends on the weld nugget size [26]. Automotive
28 manufacturers use a minimum weld size of $4\sqrt{t}$ [27-29], where t is the sheet thickness in mm; but $3.5\sqrt{t}$

or $5\sqrt{t}$ are also used [30]. It is also possible that a minimum weld size is defined for ranges in thickness and variations can be allowed for different applications [31]. For the thickness of the sheet used in the present study the range of weld nugget size would be 3.7 to 5.3 mm. Thus, the specimens in the current study would generally be acceptable in terms of the nugget size. Specimen A (Fig. 7 (a)) weld nugget size was 5.2 mm, while the weld nugget size of specimen B (Fig. 7 (b)) was 4.6 mm. In Fig. 8 the EDS maps of a similar TWIP steel joint are shown. It is evident that the cracks formed near the coating which are rich in Zn, While, the role of Zn cannot be un-ambiguously confirmed, since it was not within the scope of this study to quantify the Zn ingression into the steel substrate (which requires WDS or possible TEM analysis), the results indicate that Zn may be a factor.

3.2. Self-Piercing Riveting (SPR) technique

The range of mechanical fasteners currently available is large. Self-piercing rivets have been identified as such types of fasteners with considerable potential for use in automotive bodies. The SPR process is essentially a cold forming operation in which two or more pieces of material are mechanically fastened together. There is also no requirement, in either case, for the pre-drilling of holes in the components to be joined. The three main quality criteria of a SPR joint are: the rivet head height, the interlock distance and the minimum remaining bottom material thickness. The rivet head height is important for the cosmetic appearance, the tightness of the joints and consequently the joint strength. The minimum remaining bottom material thickness does not have large influence on the joint strength but it is important for noise, vibration and corrosion. The interlock distance is the most important joint quality, as it determines the locking strength between the rivet and the bottom sheet [25]. Regarding the SPR joints of the present study (Fig. 9), the rivet head height was the same for both dissimilar combinations (0.3 mm). The interlock distance for the TWIP/Al 5754 was 0.74 and 0.7 mm, while the corresponding values for the TWIP/Al 6111 were 0.55 and 0.52 mm. In the case of TWIP/Al 5754 the bottom thickness varied from 0.05 (close to the tip of the die) to 0.72 mm, whereas for the TWIP/Al 6111 the corresponding range was from 0.2 to 0.25 mm (tip of the die). No Zn embrittlement cracks were evident, which would suggest that Zn didn't melt during this process.

3.3. Kerb Konus Riveting (KKR) technique

In Fig. 10 the cross sections of all three combinations joined by the use of the other fastening technique of the present study (KKR) are shown. In the TWIP/TWIP joint, no cavities or cracks were observed, as opposed with the dissimilar combinations where cavities between the rivet and the TWIP sheet were evident. No cracks due to Zn melting were noted.

3.4. EJOWELD technique

EJOWELD technique is considerably new friction-weld welding process for the BIW. The EJOWELD process successfully creates this high strength joint – typically between light alloys and boron steel of

up to 1800 MPa. EJOWELD's advanced friction weld system deploys specially developed components to secure structure of assembly; a pin for single-sided fixing, and an alternative element for double sided access. The process creates no sparks or flash and very little noise whilst localising heat generation. In Fig. 11 the cross sections and IPF's of the dissimilar combinations of the present study produced by the EJOWELD technique are shown. It can be seen that grain size exhibited homogeneity throughout the samples and didn't differ significantly near the thermo-mechanically affected zone (TMAZ). Cracks were found in the EBSD and EDS maps of Fig. 11 and 12, respectively. Zinc was clearly evident at the crack as shown in Fig. 12 (d). There was no evidence of intermetallics between Fe and Al in the joint area which can be due to small amount of time for diffusion and precipitation.

3.5. Mechanical properties

In Fig. 13 the load-displacement curves for the TWIP/TWIP combination are shown. The largest maximum load and elongation at maximum load was exhibited by specimen B produced with RSW (13.11 kN and 2.15 mm, respectively), while the corresponding values for specimen A were 10.52 kN and 2.1 mm. The KKR specimen maximum load was 5.32 kN while the max elongation at maximum load was 1.42. Regarding the dissimilar TWIP/Al 5754 combination (Fig. 14), SPR showed the largest maximum load and elongation (7.43 kN and 2.66 mm), while EJOWELD came in close (6.36 kN and 2.26 mm). The KKR specimen exhibited a maximum load of 3.07 kN and elongation of 1.87 mm. Lastly, considering the TWIP/Al 6111 (Fig. 15), SPR showed the highest maximum load (6.31 kN) and second highest maximum elongation at maximum load (2.22 mm), with the corresponding values for EJOWELD being 5.81 kN and 2.06 mm, respectively. The KKR specimen's maximum load and elongation were 1.74 kN and 1.22 mm, respectively. Also, by comparing the external work of each joint, it can be seen that for the TWIP/TWIP combination, specimen A exhibited nearly double the work done compared to B (24 vs 13.3 J), while KKR came third with 4.9 J. In the case of TWIP/Al 5754, the corresponding value for SPR was 27.7 J, while EJOWELD and KKR followed with 9.5 and 4.5 J, respectively. Lastly, for the TWIP/Al 6111 combination, EJOWELD exhibited a value of 17.5 J, while SPR and KKR 9.4 and 1.6 J, respectively.

For a lap shear joint, the shear strength is governed by several factors, such as material tensile strength, tearing strength, secondary bending, and specimen configuration [19]. The key influential factor can generally be discovered by examining the failure mode of the specimen. Figure 16 shows the failure modes for the two specimens produced by RSW (A and B). Both specimens failed with the same mode, which was by interfacial nugget failure. In the case of the SPR the two dissimilar combinations failed with different modes (Fig. 17). The TWIP/Al 5754 failed by sheet pull-out, whereas the TWIP/Al 6111 by rivet pull-out failure. The KKR-produced joints failed all by the same mode which was sheet failure (Fig. 18). The structure failed by the rivet being pulled out after the deformation of the sheets. In the case of the EJOWELD dissimilar joints, they both failed by sheet pull-out failure (Fig. 19).

4. Discussion

Generally, RSW spot welds with larger sizes have larger lap shear strength values. However, the specimen A, even having a larger nugget, exhibits a lower strength than specimen B. The welding process strongly affects the nugget geometry which in turn has an influence on the RSW joint strength [5]. For the TWIP/TWIP combination in terms of lap shear strength, the specimen B of RSW exhibited the highest maximum load and maximum elongation at maximum load, while the maximum load of specimen A was approximately 20 % smaller. Also, the external work done for specimen B was nearly double than for specimen B (24 and 13.3 J, respectively). This deviation was due to the different welding cycle profiles that resulted in large differences in terms of grain size and grain orientation diversity between the two samples. Uniform grain orientations within the fusion zone contribute to an increased Taylor factor [32]. An increase in Taylor factor within the fusion zone indicates a lower tendency for slip as a result of tensile loading along the rolling direction. This may contribute to the lowered ductility observed within the fusion zone. Also, the smaller grain size contributes to higher strength of the weld, as the available room for the gliding of dislocations through the fusion zone is reduced. Due to the smaller nugget diameter, the samples in the present study had less nugget penetration, thus during testing the nuggets failed to sustain the shear load, leading to interfacial / nugget failure of the welds. Also, the chemical analysis showed LME cracking occurrence near the coating/ surface of the TWIP steel. On the other hand, the specimen produced by KKR exhibited a maximum load about 60 % smaller than specimen B. This is most possibly due to the presence of a hole in KKR which increases the stress concentration factor [33]. During lap-shear testing, the hole expands and leads to sheet failure at lower loads.

Considering the dissimilar joints in the current study the SPR-produced joints were the strongest in terms of maximum load and maximum elongation. Depending on the rivet and die combination, it can generally be assumed that the greater the interlock - the higher the joint strength. The TWIP/Al 5754 failed by sheet pull-out, while the TWIP/Al 6111 by rivet pull-out mode, owing to the difference of the Al sheets thicknesses, which could be suggested that is the reason for the large difference regarding the external work done (27.7 J for the TWIP/Al 5754 9.4 J for the TWIP/Al 6111). In this situation (rivet pull-out and sheet pull-out), it is the interlock between the rivet and the bottom sheet that applies the compression at the joint area and determines the joint strength. The interlock distance was larger in in the TWIP/Al 5754 than in TWIP/Al 6111. The dissimilar joints produced by EJOWELD were closely second to the SPR in terms of maximum load. Their texture was found to be homogeneous, as opposed with the RSW joints where due to the largest temperatures that were developed, the grain size in the fusion zone was significantly larger than in the base metal. Comparing the similar and dissimilar joints produced by different techniques in the present study, the former show slightly better mechanical properties, owing primarily to the sheet thickness difference between Al 5754 (2 mm) and Al 6111 (1.12 mm).

In the dissimilar joints produced with EJOWELD, no Fe-Al intermetallics were evident at the joint area. The samples failed by sheet pull-out mode which suggested that their strength depended on length of the heat affected zone between the sheets. The temperature changes during the process are not expected to melt the matrix material and the micro-structural changes are therefore attributed to recrystallization. No evidence of formation of intermetallic were found in the SEM analysis. Also, it could be suggested the lap shear strength, max elongation and external work of the joints would depend on the solidification cracks forming near the fusion zone. Finally, the KKR-produced dissimilar joints exhibited the lowest maximum load, elongation and external work of all the techniques used in the present study and considering their failure mode (sheet failure), it can be deduced that the governing parameter for the joint strength would be the sheet strength. In the case of SPR, the compression load between the sheets is higher in comparison to KKR. Also, the SPR rivet exhibits a more complicated geometry, while it pierces the sheets without creating an actual hole, as opposed to the KKR. This results in higher shear load and maximum elongation during lap-shear tests.

5. Conclusions

In the current work, RSW, SPR, KKR and EJOWELD techniques were compared in terms of mechanical properties. To the best of the authors' knowledge it is the first time the KKR and EJOWELD methods were compared to conventional joining methods. A relationship between the joint properties, the mechanical performance (maximum load and elongation) and failure mode was established for all samples. For the TWIP/TWIP combination in terms of lap shear strength, specimen B of RSW exhibited the highest load and elongation, while the maximum load of specimen A was approximately 20 % smaller. The RSW joints failed by interfacial mode. On the other hand, the specimen produced by KKR exhibited a maximum load about 60 % smaller than specimen B, because of the presence of the hole which raised the stress concentration factor. Considering the dissimilar joints, the SPR-produced joints exhibited the highest load and elongation. The TWIP/Al 5754 failed by sheet pull-out, while the TWIP/Al 6111 by rivet pull-out mode, as Al 6111 had smaller thickness resulting in a lower interlock distance. The dissimilar joints produced by EJOWELD were closely second to the SPR in terms of maximum load. Their texture was found to be homogeneous, as opposed to the RSW joints where the grain size in the fusion zone was significantly larger than in the base metal. The EJOWELD joints failed by sheet pull-out mode which depended on length of the fusion zone between the sheets. The KKR-produced dissimilar joints exhibited the lowest maximum load and elongation of all techniques under this study.

Acknowledgements:

The funding of this project and the supply of the materials and data by POSCO is gratefully acknowledged**.**

1

2

3

References

[1] R.W. Crandall, Policy watch: corporate average fuel economy standards, J. Econ. Perspect., 6 (1992) 171-180.

[2] C. Action, Reducing CO2 emissions from passenger cars, URL: http://ec. europa. eu/clima/policies/transport/vehicles/cars/index_en. htm, (2012).

[3] I. Polmear, Light alloys, Third ed., Arnold, 1995.

[4] G.L. Leone, K. Ban, The 2nd generation Audi space frame of the A2: A trendsetting all-aluminium car body concept in a compact class car, in: FISITA World automotive congress, Seoul, Korea, 2000.

[5] L. Han, M. Thornton, M. Shergold, A comparison of the mechanical behaviour of self-piercing riveted and resistance spot welded aluminium sheets for the automotive industry, Mater. Des., 31 (2010) 1457-1467.

[6] P. Briskham, N. Blundell, L. Han, R. Hewitt, K. Young, D. Boomer, Comparison of self-pierce riveting, resistance spot welding and spot friction joining for aluminium automotive sheet, in, SAE Technical Paper, 2006.

[7] G. Koenig, R. Koehr, F. Kybart, S. Walter, J. Catterall, J. Krumbach, R. Heyll, A. Wolf, Designing and producing lightweight automobile bodies, in, Google Patents, 1998.

[8] D. Carle, G. Blount, The suitability of aluminium as an alternative material for car bodies, Mater. Des., 20 (1999) 267-272.

[9] W.S. Miller, L. Zhuang, J. Bottema, A.J. Wittebrood, P. De Smet, A. Haszler, A. Vieregge, Recent development in aluminium alloys for the automotive industry, Mater. Sci. Eng. A, 280 (2000) 37-49.

[10] O. Bouaziz, S. Allain, C.P. Scott, P. Cugy, D. Barbier, High manganese austenitic twinning induced plasticity steels: A review of the microstructure properties relationships, Curr. Opin. Solid State Mater. Sci., 15 (2011) 141-168.

[11] O. Bouaziz, N. Guelton, Modelling of TWIP effect on work-hardening, Mater. Sci. Eng. A, 319–321 (2001) 246-249.

[12] D. Barbier, N. Gey, S. Allain, N. Bozzolo, M. Humbert, Analysis of the tensile behavior of a TWIP steel based on the texture and microstructure evolutions, Mater. Sci. Eng. A, 500 (2009) 196-206.

[13] C. Beal, X. Kleber, D. Fabregue, M. Bouzekri, Liquid zinc embrittlement of twinning-induced plasticity steel, Scripta Mater., 66 (2012) 1030-1033.

[14] L. Agudo, D. Eyidi, C.H. Schmaranzer, E. Arenholz, N. Jank, J. Bruckner, A.R. Pyzalla, Intermetallic Fe x Al y -phases in a steel/Al-alloy fusion weld, J. Mater. Sci., 42 (2007) 4205-4214.

[15] S. Aslanlar, The effect of nucleus size on mechanical properties in electrical resistance spot welding of sheets used in automotive industry, Mater. Des., 27 (2006) 125-131.

[16] D.R. Boomer, J.A. Hunter, D.R. Castle, A new approach for robust high-productivity resistance spot welding of aluminium, in, SAE Technical Paper, 2003.

[17] Y. Cho, S.J. Hu, W. Li, Resistance spot welding of aluminium and steel: A comparative experimental study, Proc. Inst. Mech. Eng., B J. Eng. Manuf., 217 (2003) 1355-1363.

[18] Y. Abe, T. Kato, K. Mori, Joinability of aluminium alloy and mild steel sheets by self piercing rivet, J. Mater. Process. Technol., 177 (2006) 417-421.

[19] Y. Abe, T. Kato, K. Mori, Self-piercing riveting of high tensile strength steel and aluminium alloy sheets using conventional rivet and die, J. Mater. Process. Technol., 209 (2009) 3914-3922.

[20] M. Carandente, Experimental and numerical investigation of temperature during SPR joining, in: Warwick Manufacturing Group, University of Warwick, 2016.

[21] G. Donhauser, Punching, stamping rivet, in, Google Patents, 2003.

[22] M. Maiwald, J. Thiem, Joining without a Pilot Hole using Friction Welding, ATZproduktion worldwide, 5 (2012) 10-17.

[23] S. Allain, J.-P. Chateau, O. Bouaziz, S. Migot, N. Guelton, Correlations between the calculated stacking fault energy and the plasticity mechanisms in Fe–Mn–C alloys, Mater. Sci. Eng. A, 387 (2004) 158-162.

[24] H. Kang, L. Cho, C. Lee, B.C. De Cooman, Zn Penetration in Liquid Metal Embrittled TWIP Steel, Metal. Mat. Trans. A, 47 (2016) 2885-2905.

[25] D. Li, A. Chrysanthou, I. Patel, G.J. Williams, Self-piercing riveting-a review, (2016).

[26] Y.J. Chao, Failure mode of spot welds: Interfacial versus pullout, Sci. Technol. Weld. Joining, 8 (2003) 133-137.

[27] Specification for automotive weld quality – Resistance spot welding of steel, AWS D8.1M:2007 (2007).
[28] S. Westgate, in: W. Zhang, P. Xu (Eds.) Proceedings of the 3rd International Seminar on Advances in Resistance Welding, Berlin, Germany, pp. 8-17.
[29] J.K. Larsson, J. Lundgren, E. Asbjörnsson, H. Andersson, Extensive Introduction of Ultra High Strength Steels Sets New Standards for Welding in the Body Shop, WELD WORLD, 53 (2009) 4-14.
[30] H. Zhang, J. Senkara, Resistance welding, fundamentals and applications, Taylor and Francis, 2006.
[31] N. den Uijl, F. Azakane, S. Kilic, V. Docter, Performance of Tensile Tested Resistance Spot and Laser Welded Joints at Various Angles, WELD WORLD, 56 (2012) 143-152.
[32] S. Turnage, K. Darling, M. Rajagopalan, W. Whittington, M. Tschopp, P. Peralta, K. Solanki, Quantifying structure-property relationships during resistance spot welding of an aluminum 6061-T6 joint, arXiv preprint arXiv:1605.04251, (2016).
[33] H.L. Ewalds, R.J.H. Wanhill, Fracture mechanics, Edward Arnold, 1984.

Figures

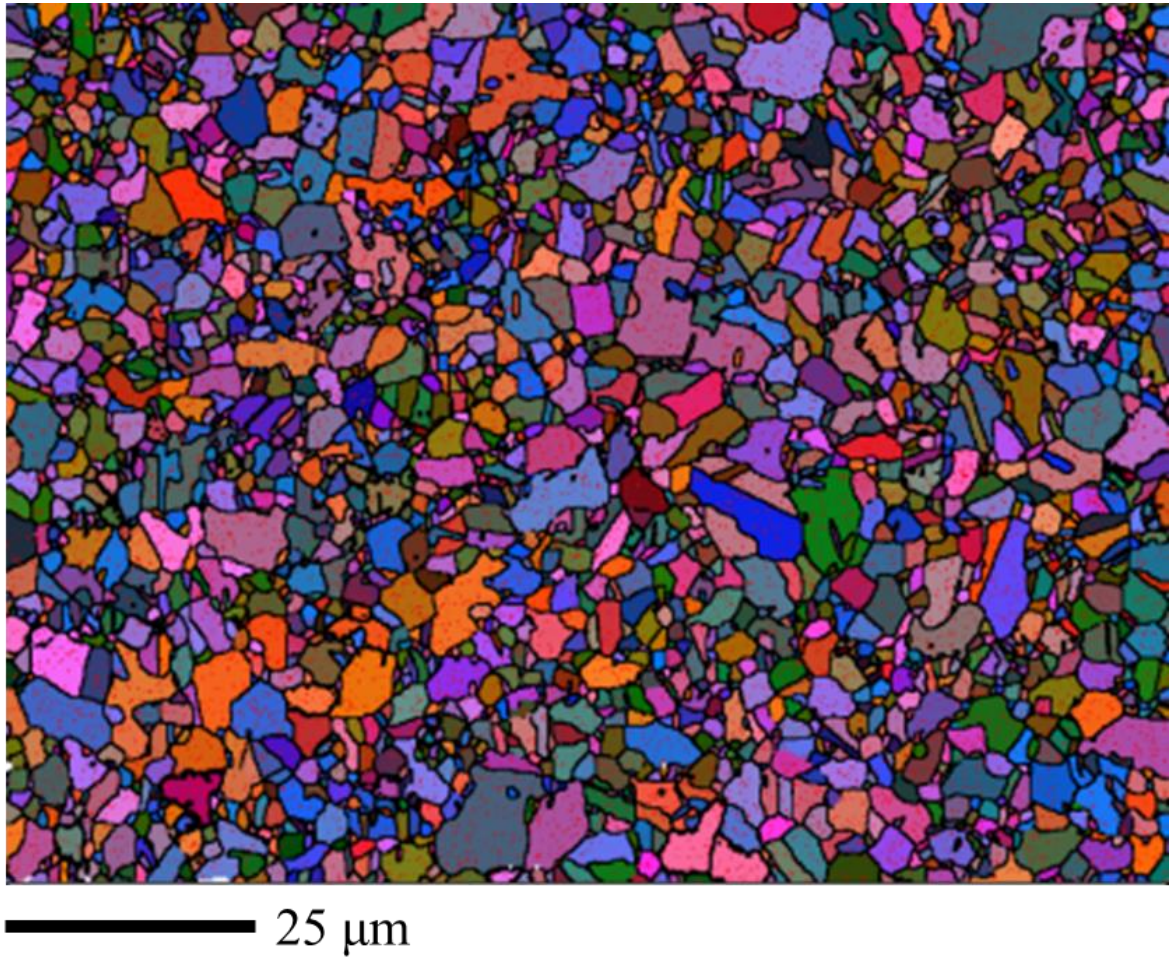

Figure 1. EBSD micrograph of the microstructure of TWIP steel prior to welding.

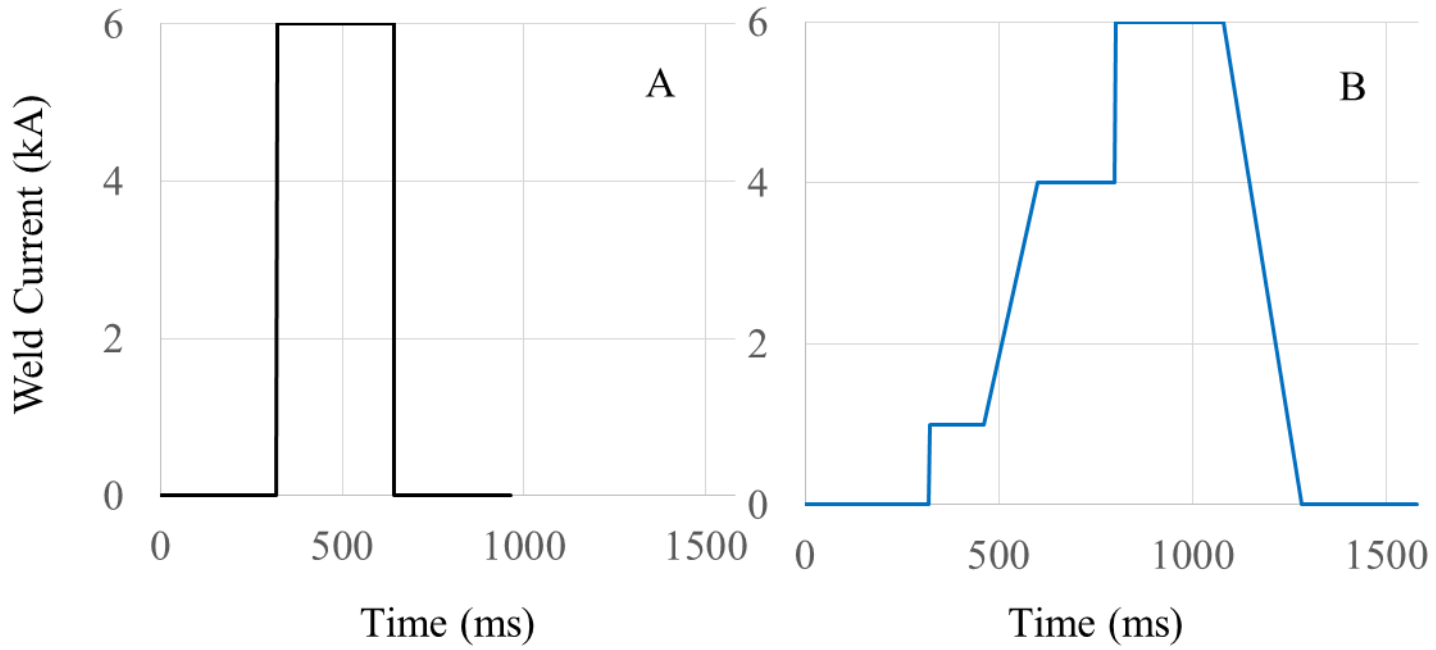

Figure 2. Welding cycle profiles for specimens A and B.

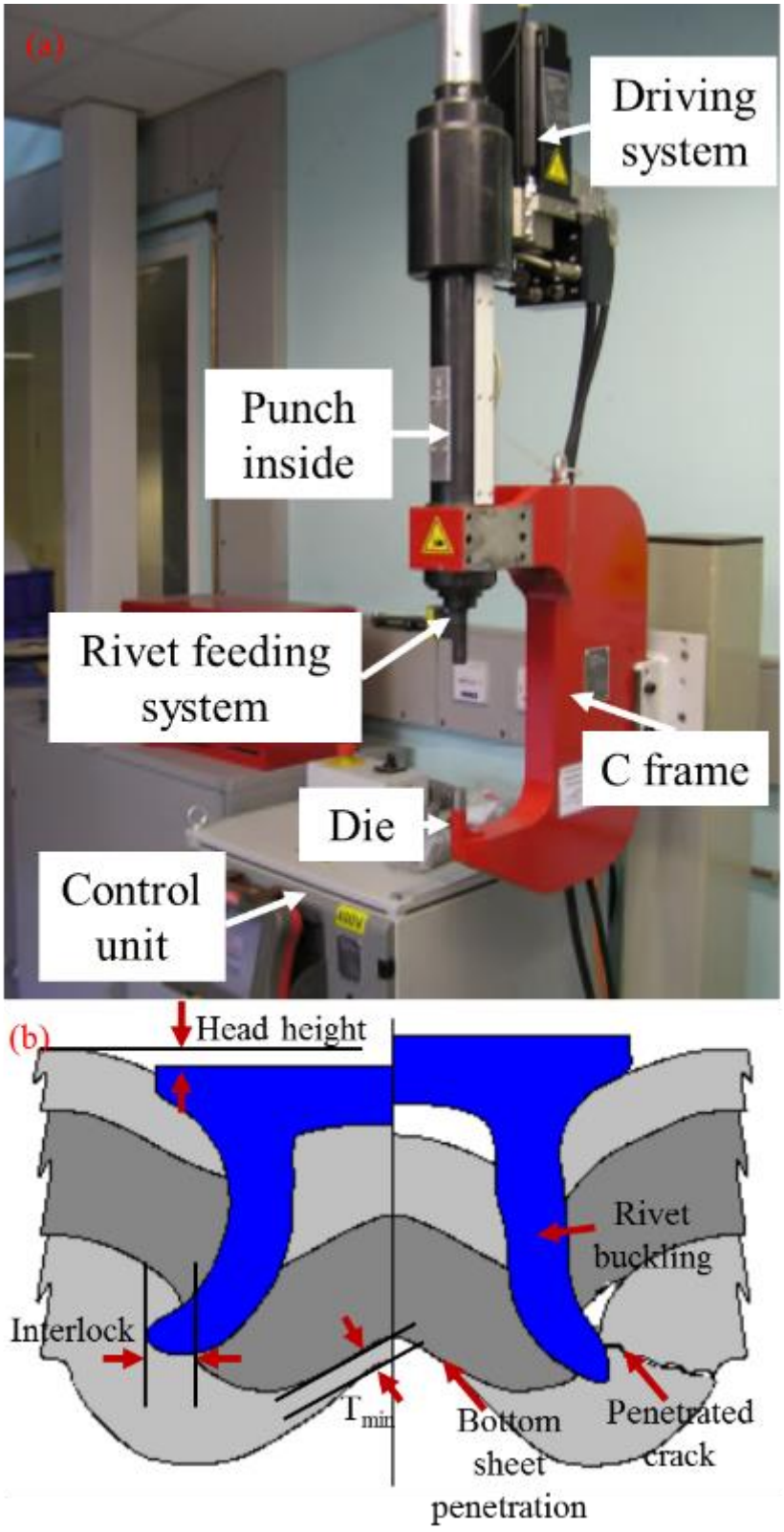

Figure 3. The system used for the production of the SPR joints in the present study (a) and quality and faults of a SPR joint (b).

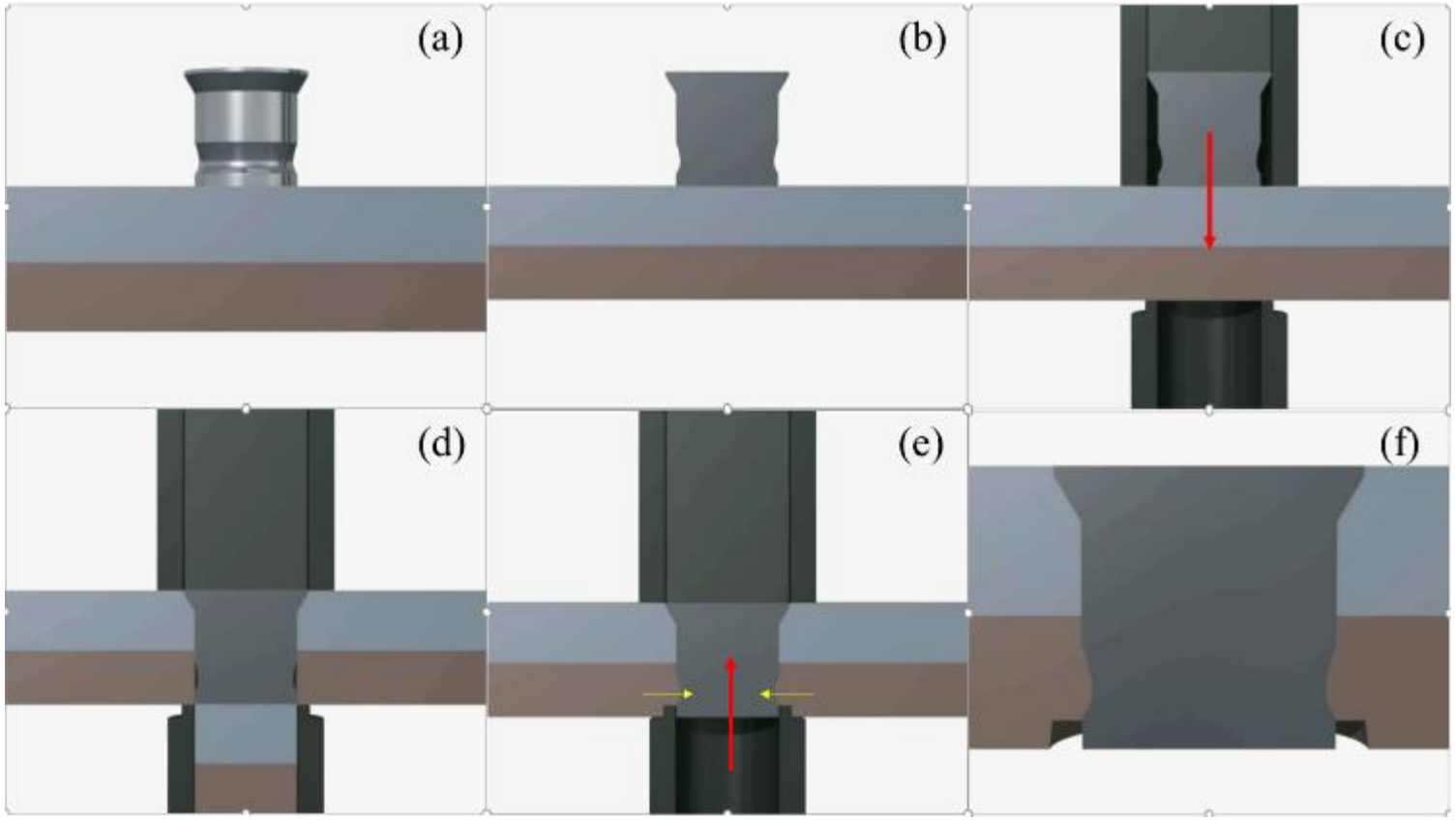

Figure 4. The Kerb Konus Tuk rivet process: rivet above top sheet (a,b), rivet punching through the top and bottom sheet (c), sheet material expulsion (d), die insertion at bottom sheet (e) and final joint (f).

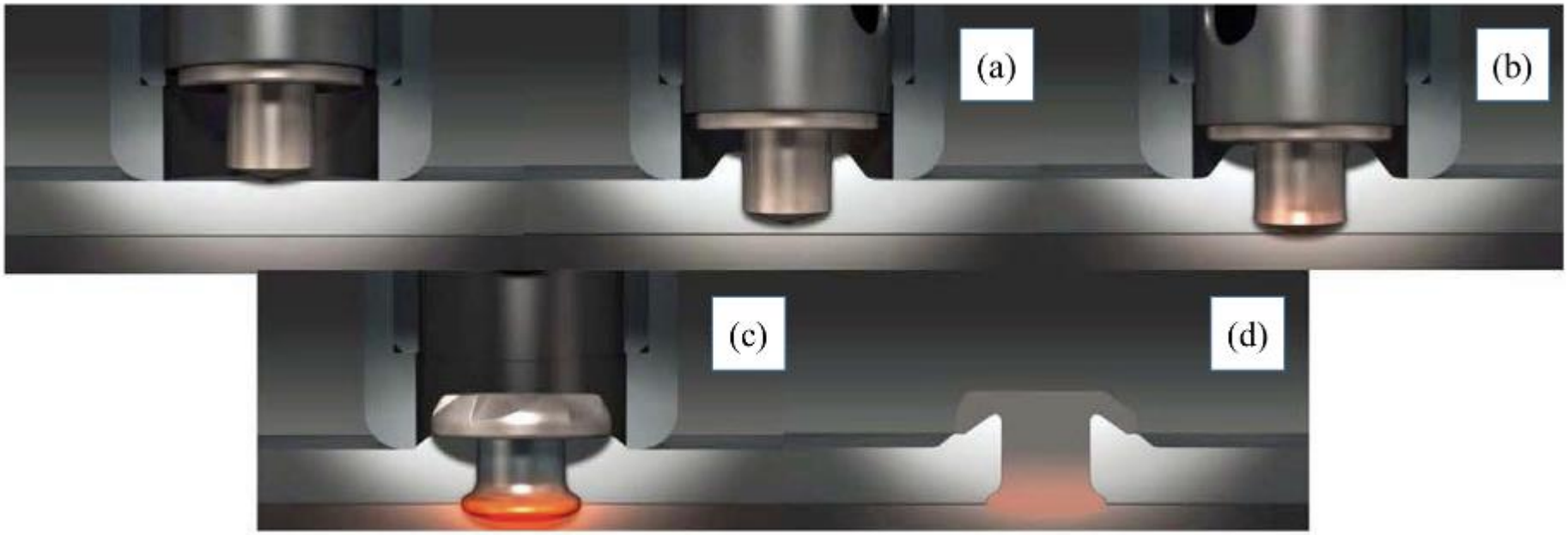

Figure 5. The EJOWELD process: rivet drilling the top sheet (a), rivet revolution (b), rivet fusion with the bottom sheet (c) and final joint (d).

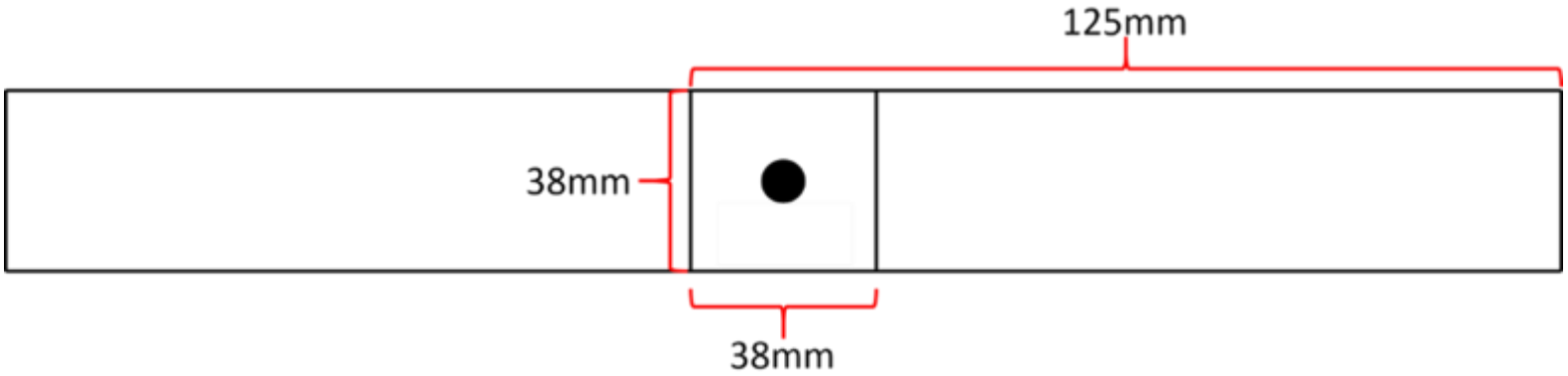

Figure 6. Lap shear test specimen coupons geometry (AWS D8).

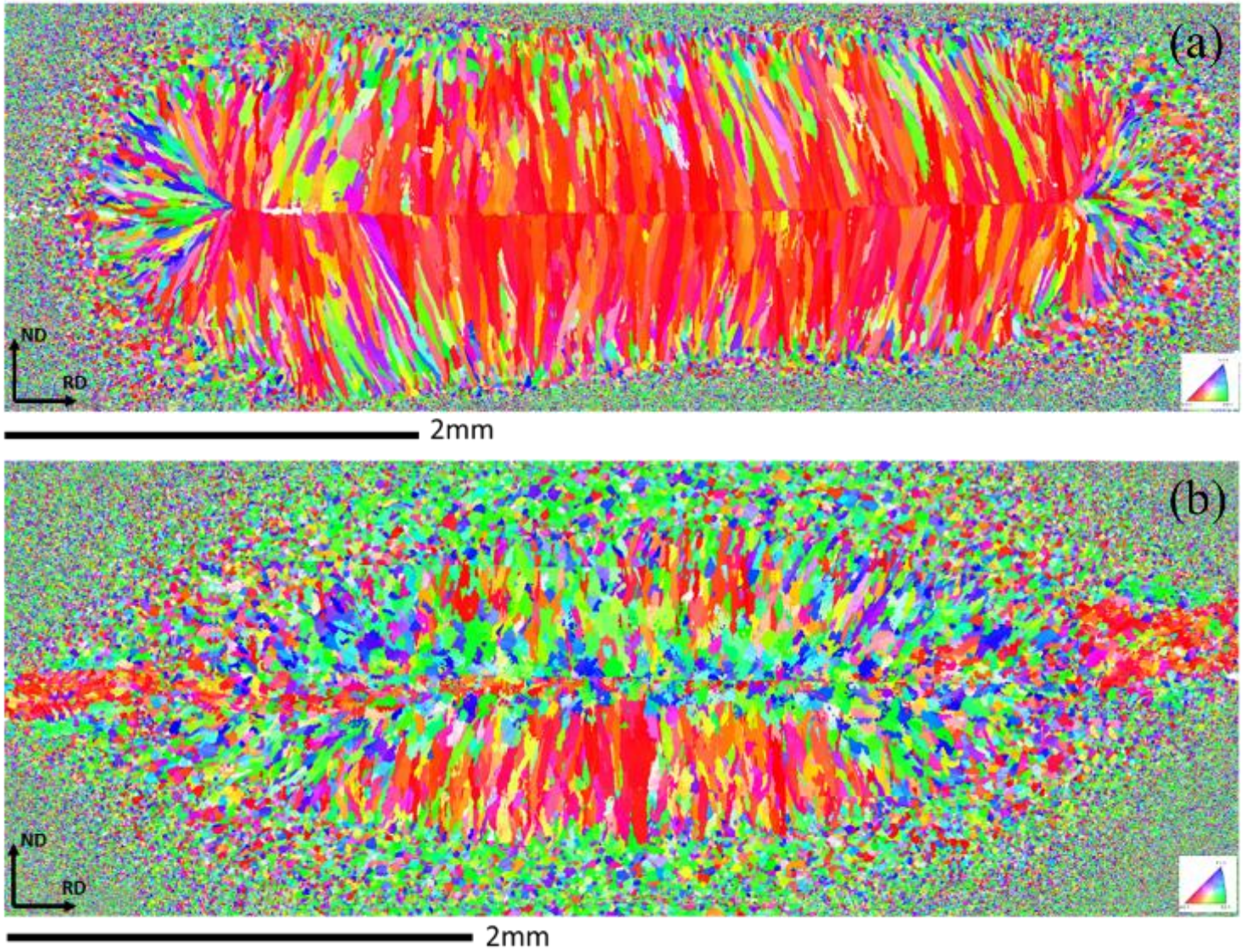

Figure 7. The Inversed Pole Figures (IPF) of the RSW A (a) and B (b) specimens.

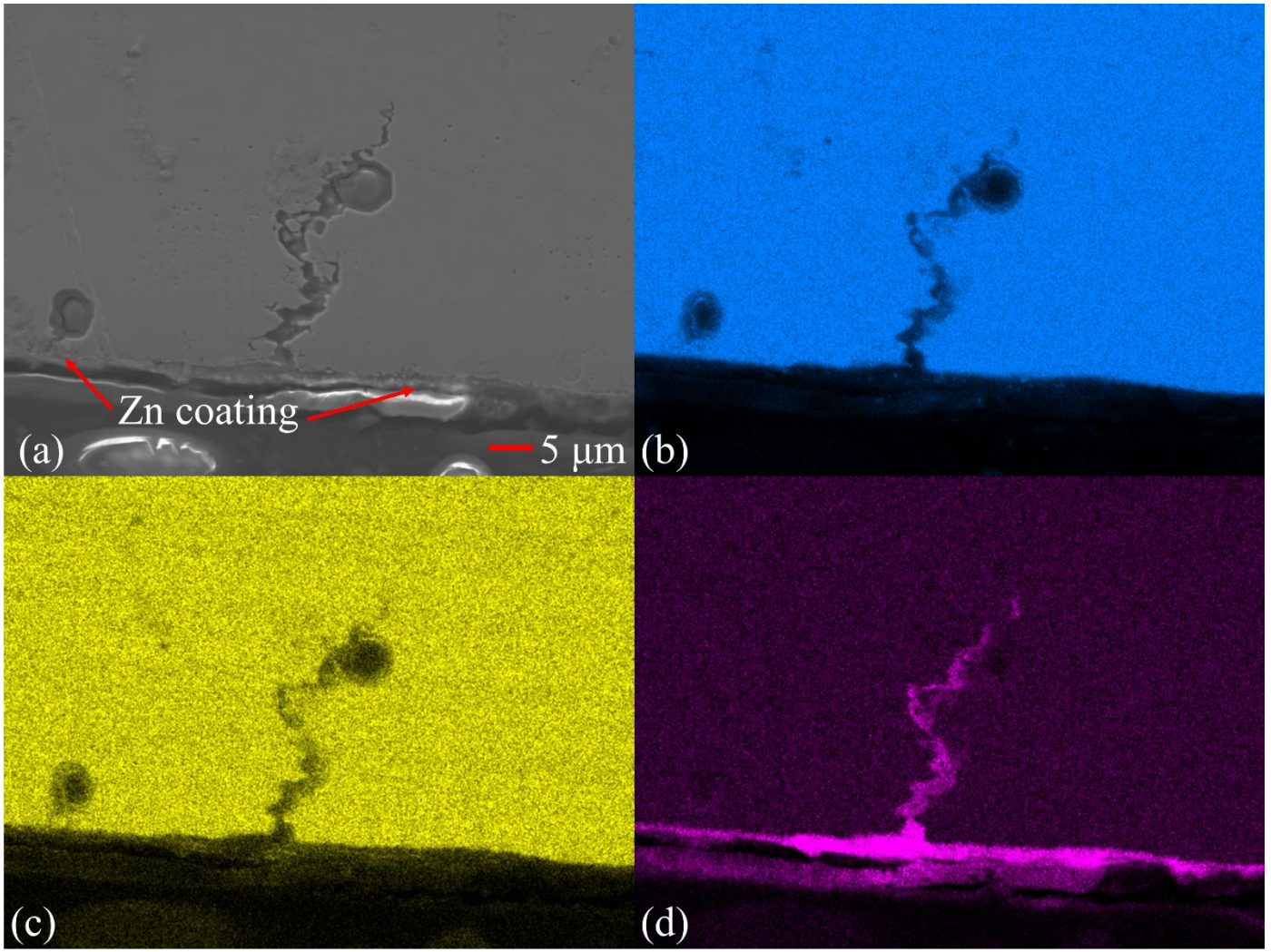

Figure 8. Cracking occurrence between the similar RSW joints: electron microscopy image (a) and EDS maps of Fe (b), Mn (c) and Zn (d).

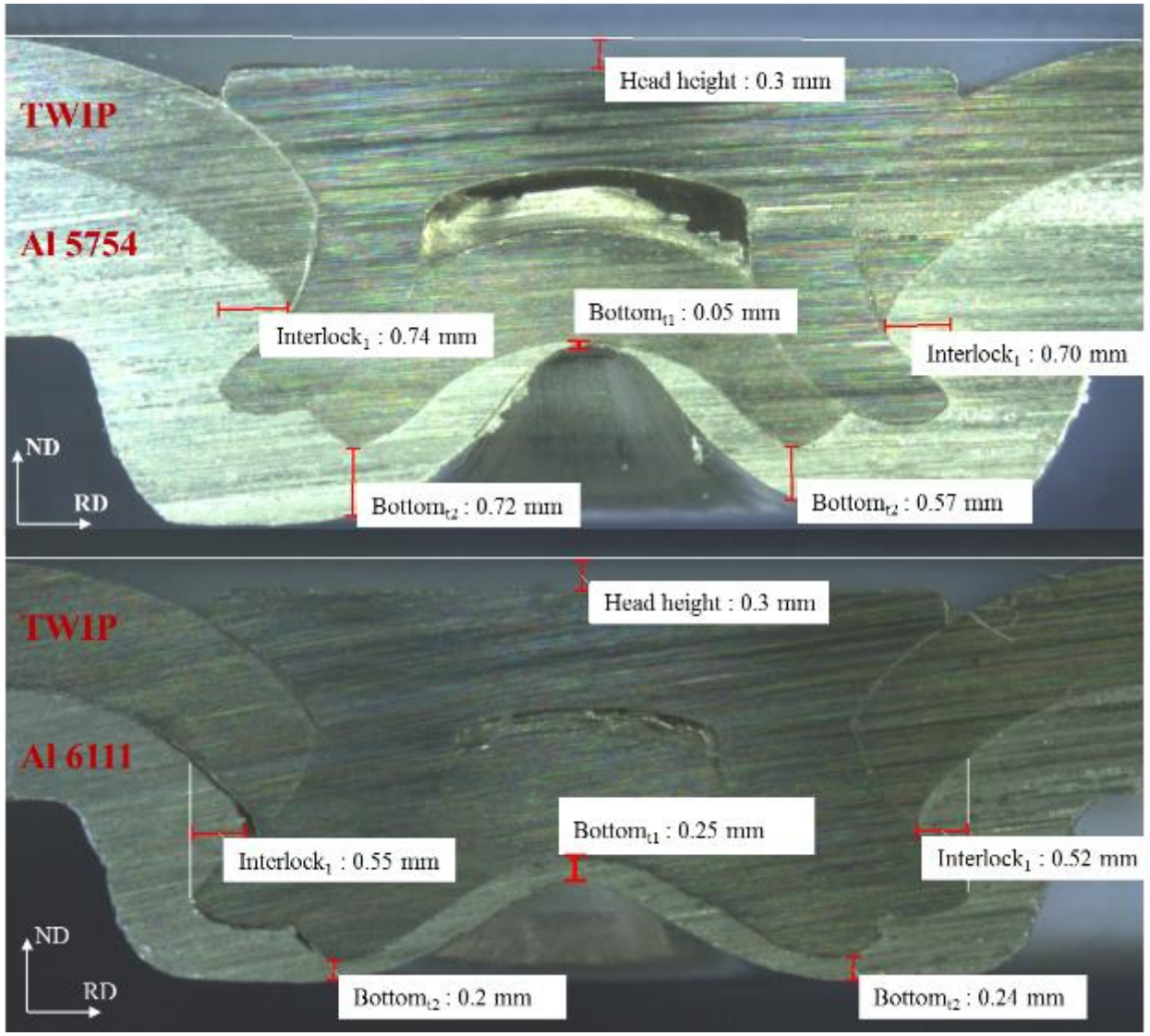

Figure 9. SPR joint quality measurements for the TWIP/Al 5754 and TWIP/Al 6111.

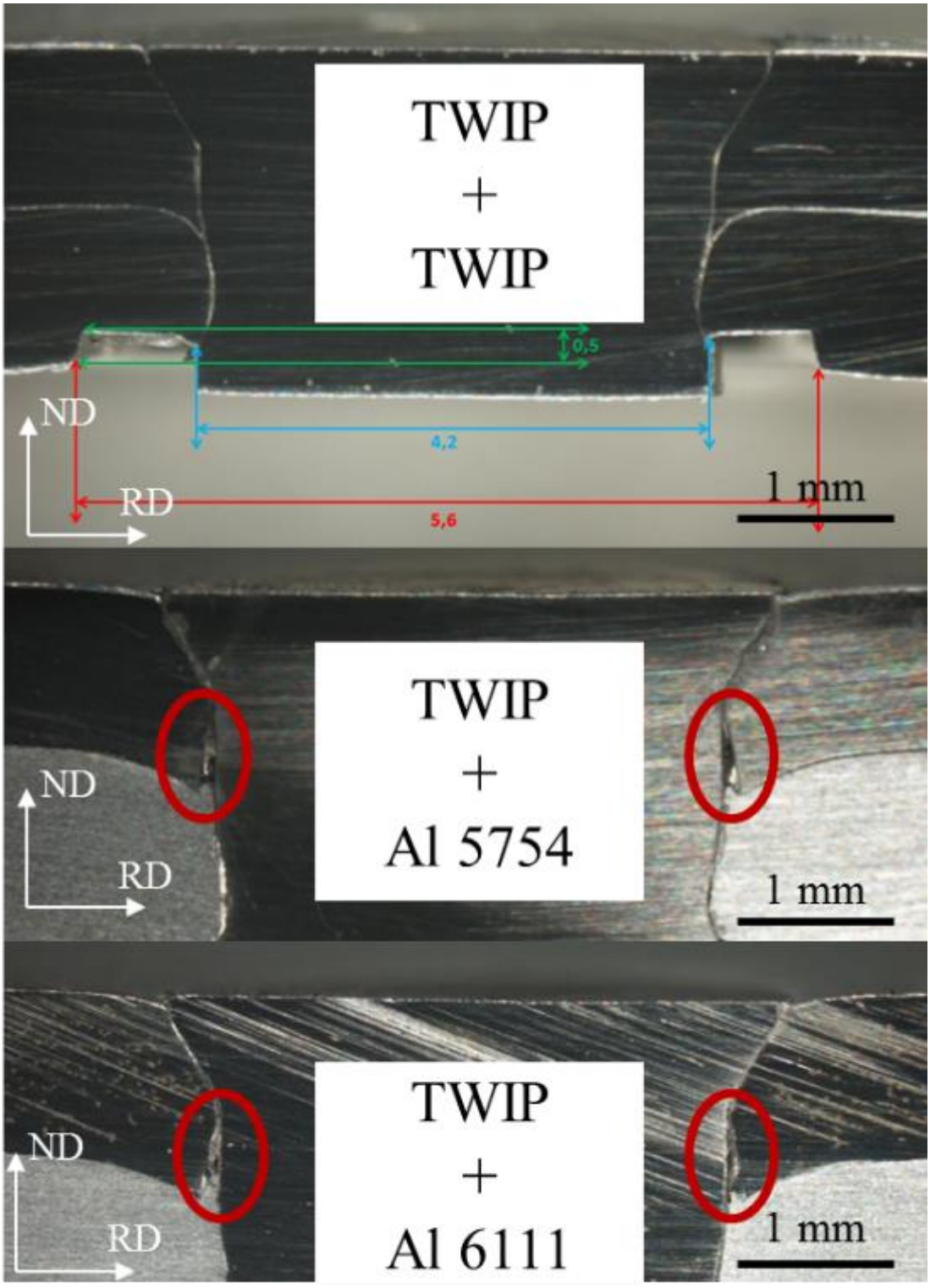

Figure 10. Cross sections of all three combinations joined by the use of KKR.

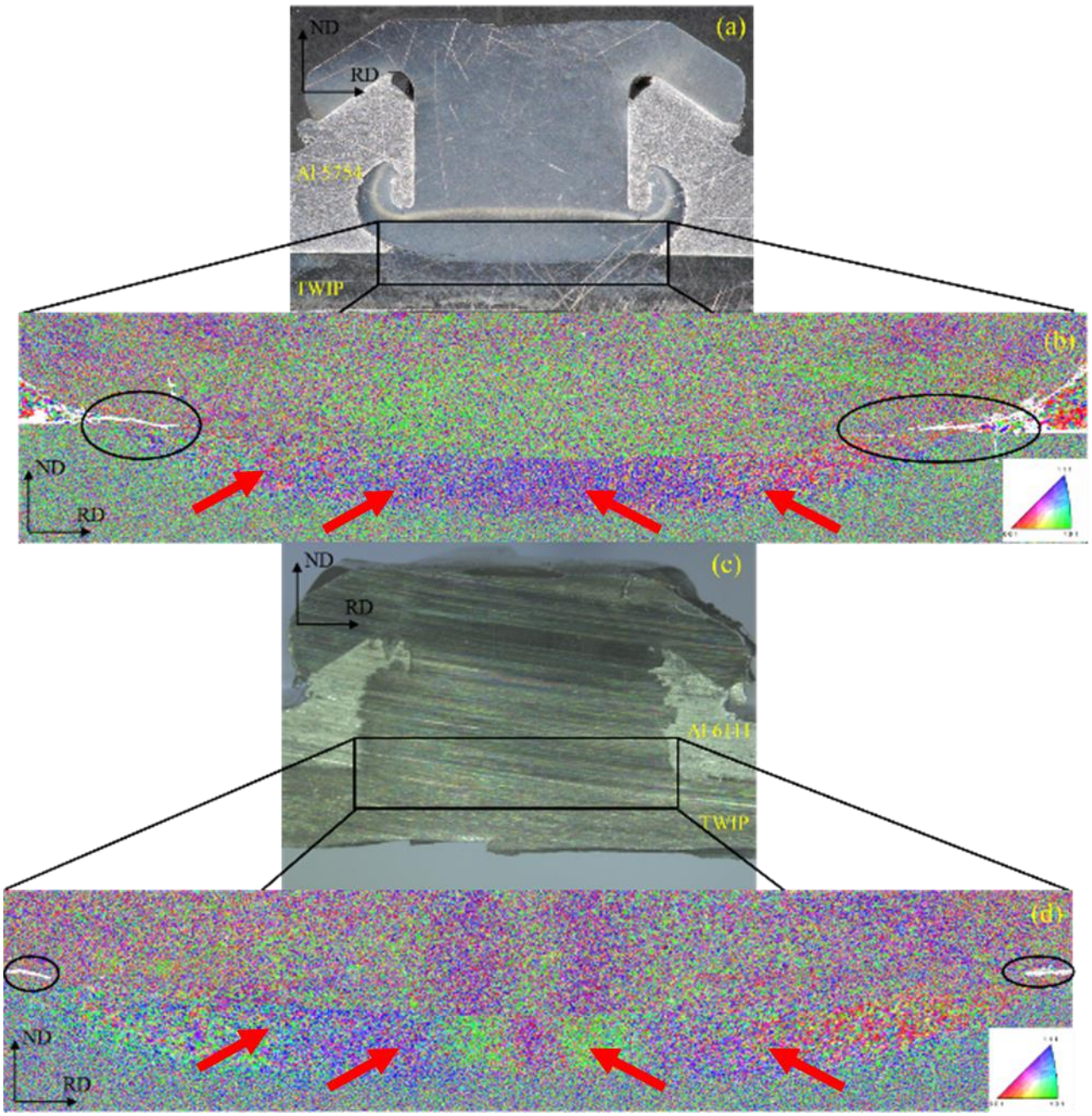

Figure 11. Cross section (a) and IPF map (b) of TWIP/Al 5754 and cross section (c) and IPF map (d) of TWIP/Al 6111 produced with the EJOWELD method. The red arrows indicate the thermo-mechanically affected zone (TMAZ).

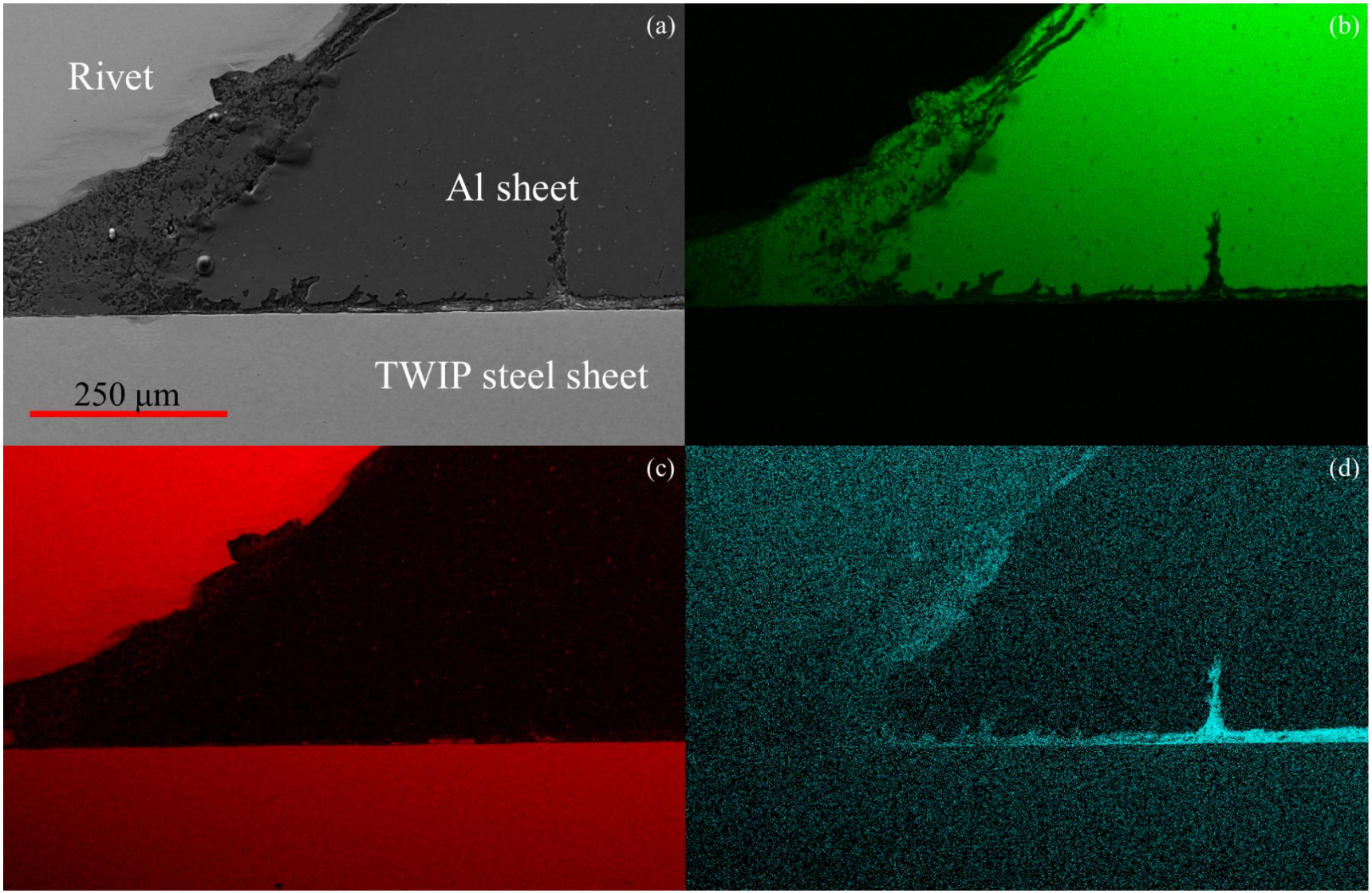

Figure 12. EDS elemental maps for a typical EJOWELD sample: electron microscopy image (a), Al (b), Fe (c) and Zn (d) map.

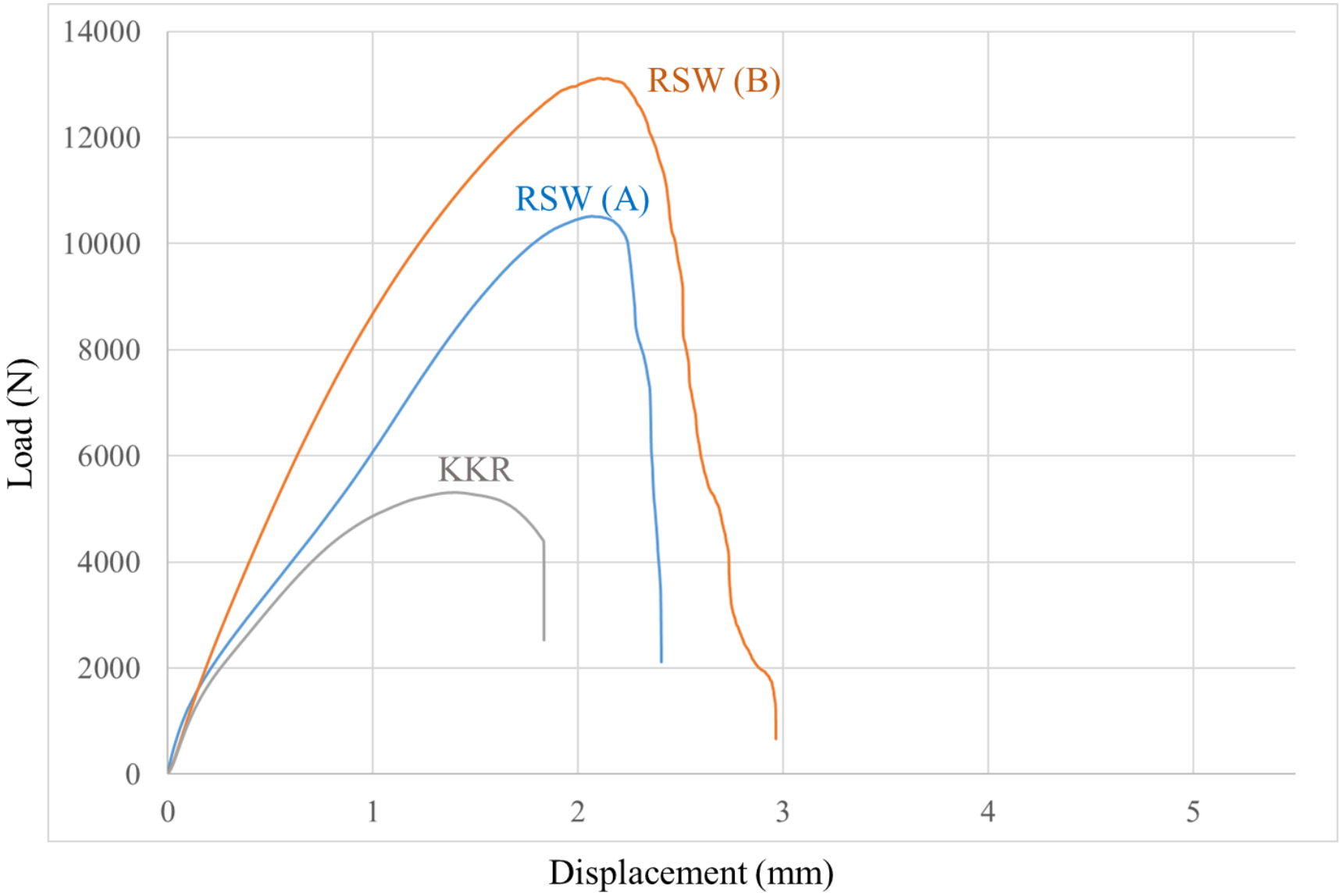

Figure 13. Load-displacement curves for the TWIP/TWIP combination.

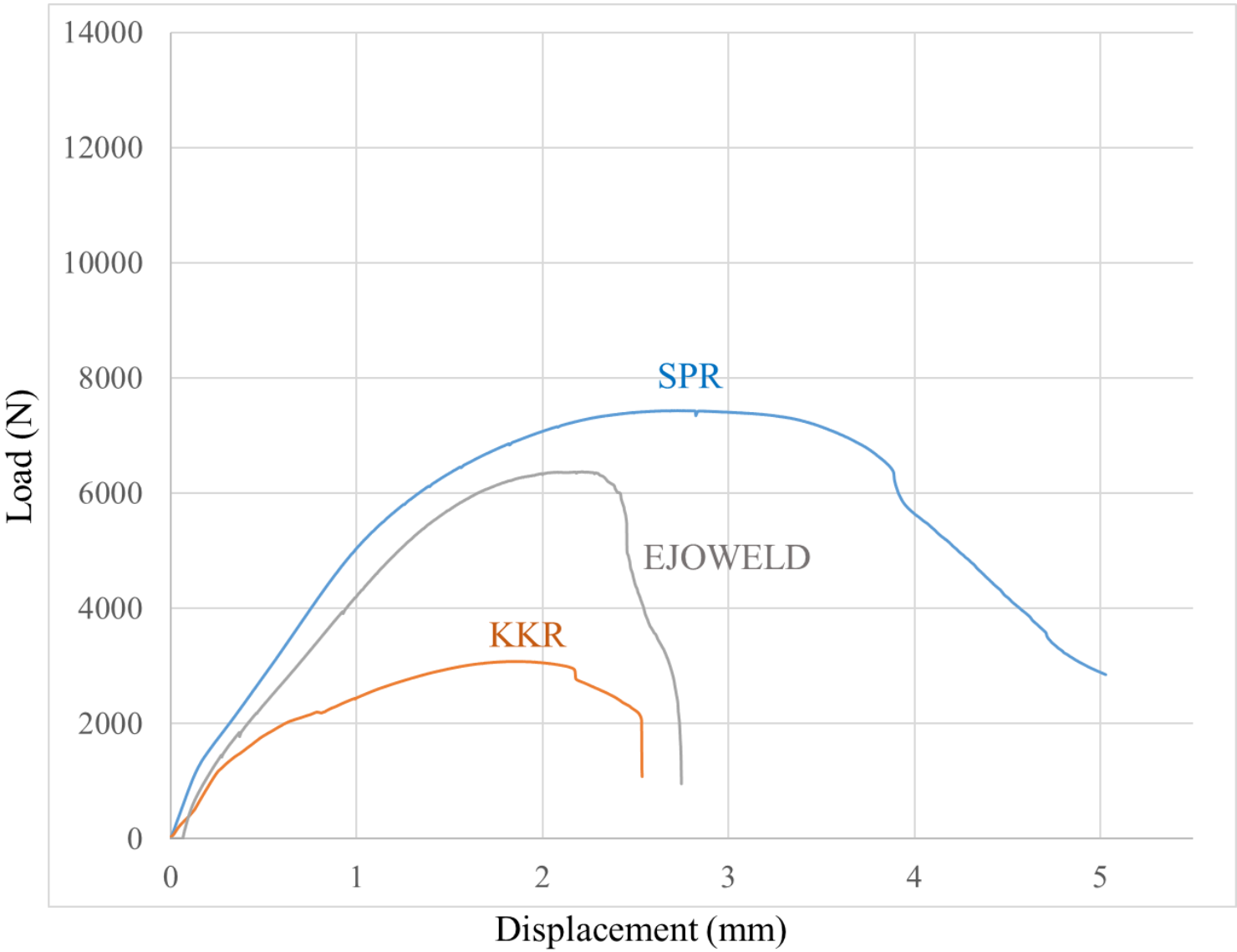

Figure 14. Load-displacement curves for the TWIP/Al 5754 combination.

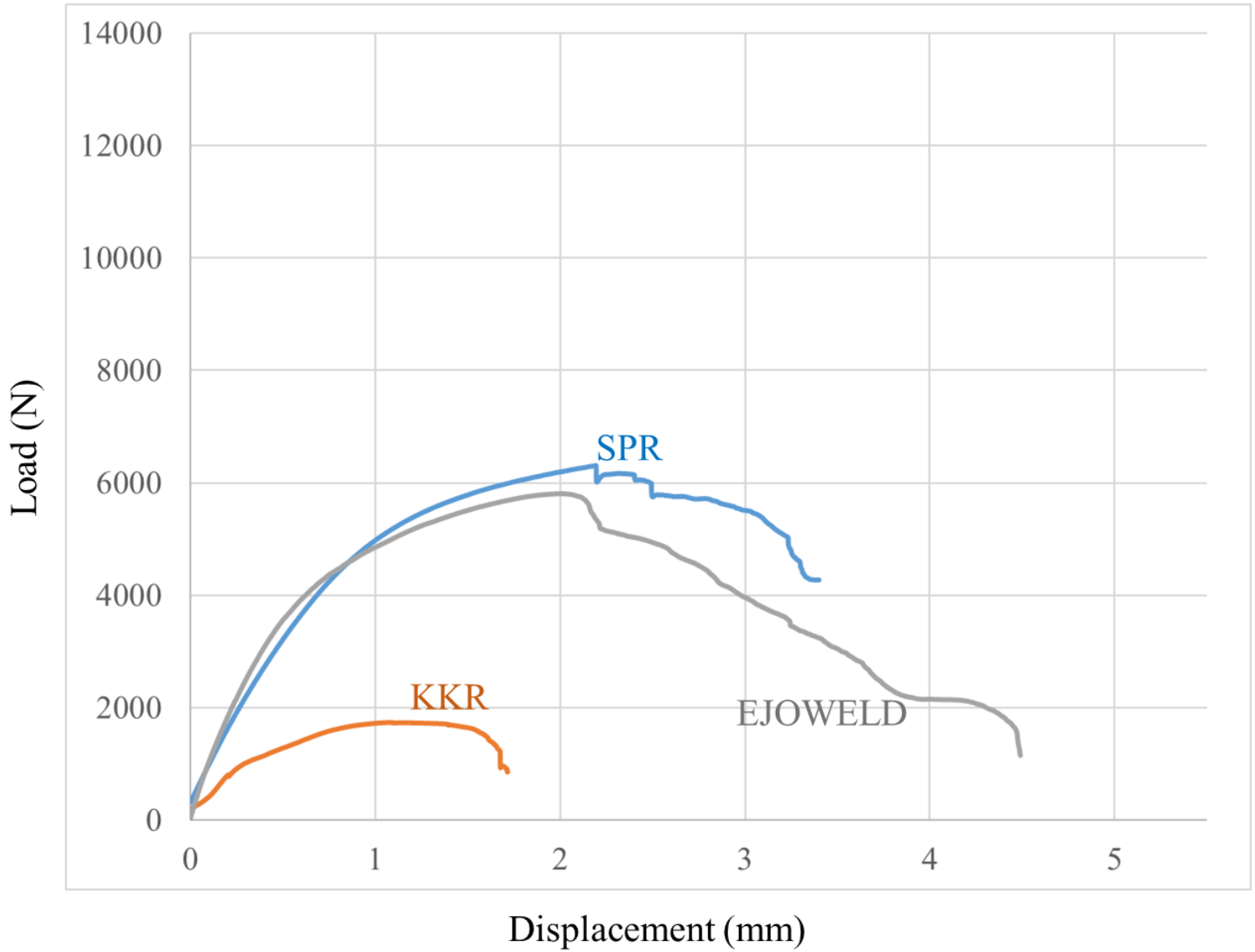

Figure 15. Load-displacement curves for the TWIP/Al 6111 combination.

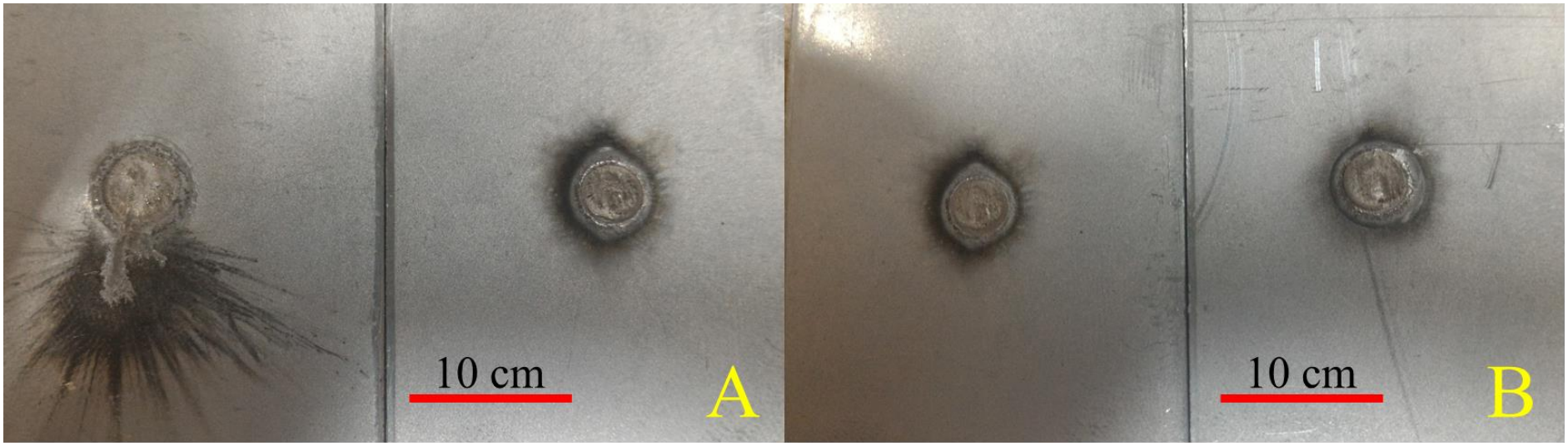

Figure 16. Failure modes for the two specimens produced by RSW (A and B)

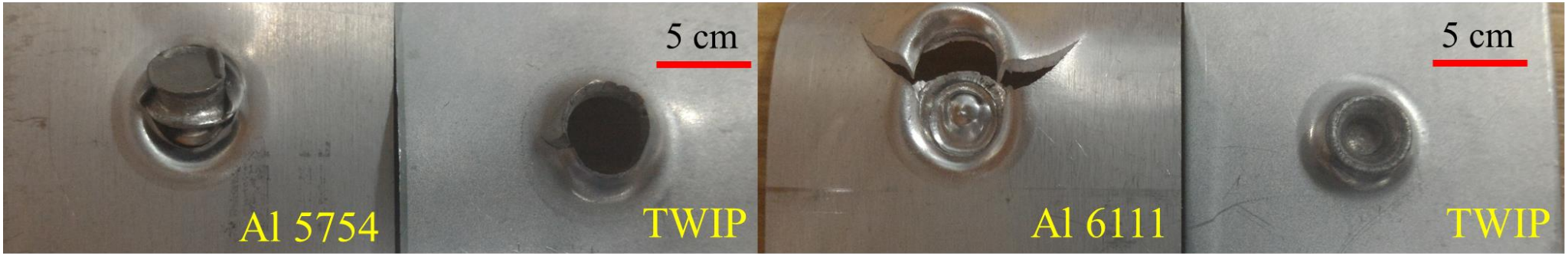

Figure 17. SPR dissimilar joints failure modes

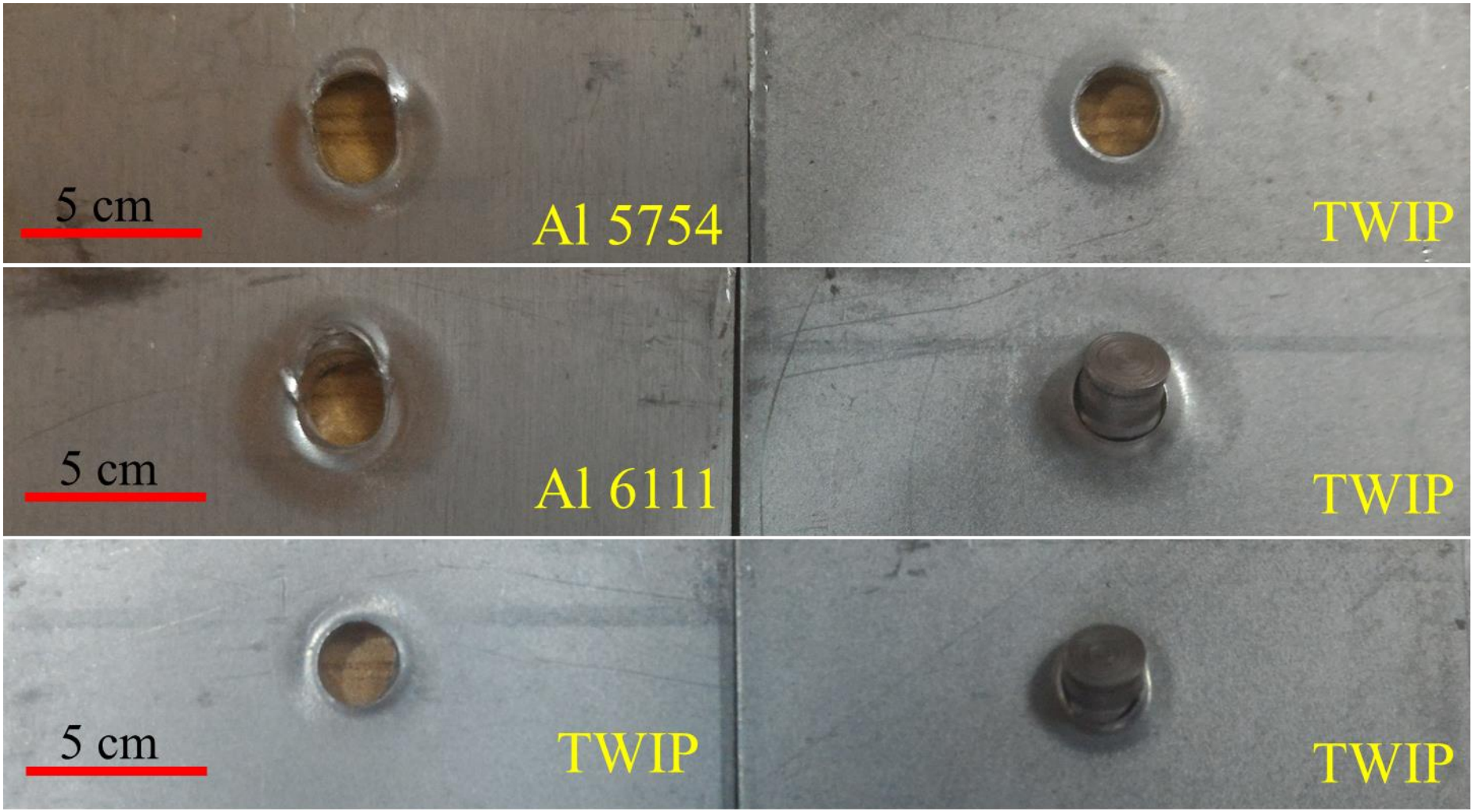

Figure 18. Kerb Konus failure modes.

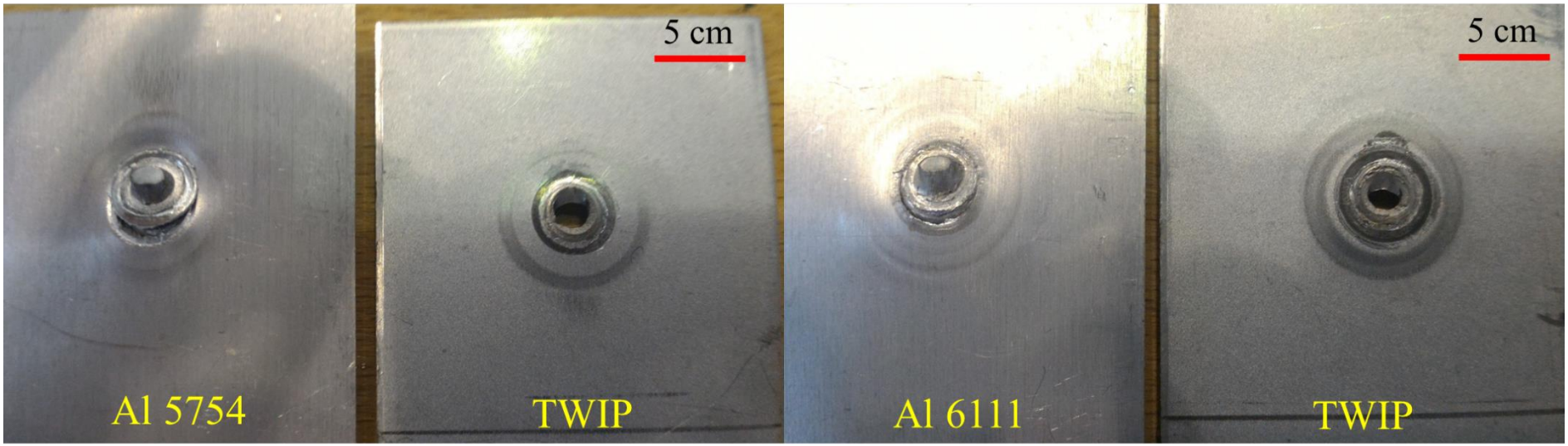

Figure 19. EJOWELD failure modes.